Hindawi
Advances in Civil Engineering
Volume 2021, Article ID 6655400, 20 pages
https://doi.org/10.1155/2021/6655400

Research Article

Seismic Energy Response of SDOF Systems Subjected to Long-Period Ground Motion Records

Yu Cheng,[1] Yao-Rong Dong,[1,2] Li Qin,[1] Yuan-Yuan Wang,[1] and Ye-Xue Li[1]

[1]*Hubei Key Laboratory of Power System Design and Test for Electrical Vehicle, Hubei University of Arts and Science, Xiangyang 441053, China*
[2]*Key Laboratory of C&PC Structures of the Ministry of Education, Southeast University, Nanjing 210096, China*

Correspondence should be addressed to Yao-Rong Dong; yaorong099@163.com

Received 23 November 2020; Revised 3 March 2021; Accepted 10 March 2021; Published 23 March 2021

Academic Editor: Luigi Aldieri

To provide an important reference for the energy-based seismic design of long-period structures, the elastoplastic dynamic analysis program is employed to study the seismic energy response of single-degree-of-freedom (SDOF) systems under two types of typical long-period ground motions. Then, the influencing relationships of external and internal factors on the energy response spectra under near-fault pulse-like and far-field harmonic ground motions are analyzed one by one. Study results are obtained as follows: within the whole period, all the input energy, hysteretic energy and damping energy spectra of SDOF systems under near-fault pulse-like and far-field harmonic ground motions, are larger than those under common ground motions, even the seismic energy response under far-field harmonic ground motions is larger than that under near-fault pulse-like ground motions. From the aspect of energy concept, the energy response spectra and energy distribution rule of SDOF systems are evaluated based on the intensity and spectral distribution under near-fault pulse-like and far-field harmonic ground motions. If the ratio of hysteretic energy to input energy (RHEIE) is determined, the hysteretic energy which must be dissipated by a structure would be derived by the method of energy-based design. The input energy and hysteretic energy are mainly influenced by damping ratio and ductility coefficient, while the yield stiffness ratio exerts minor effects. It indicates that reasonable structural design parameters would contribute to the hysteretic energy of a structure itself.

1. Introduction

It has been found that there are long-period components with the extensive study on the characteristic of earthquake records [1–3]. With the development of high-rise structures, the earthquake records whose long-period components are rich would inevitably bring the resonance effect on these tall buildings with long vibration period. For example, the dynamic behavior of high-rise buildings under various long-period ground motions should be taken into account on the seismic design of the structure. The analytical results on test specimen subjected to long-period ground motions show that the cumulative ductility is four times greater than the design value, while the maximum story drift is almost the same as the design value [4]. The base-isolated high-rise buildings with long vibration period are easily in resonance with long-period components of earthquake records in Japan. The seismic design on these tall buildings with long vibration periods must be taken seriously [5]. Particularly, the effects of near-fault long-period ground motions on the nonlinear response of base-isolated long-period structures have been noticed in recent years [6, 7]. In short, the above situations about the effects on long-period structures subjected to long-period ground motions should not be ignored easily.

Currently, due to the simplicity of force and displacement conception in the engineering practice applications, the design methods based on force and displacement parameters have been discussed and applied over the past few decades [8–11]. However, these methods would not be applicable to the inelastic seismic design of buildings located in high-intensity seismic area. Housner [12] firstly proposed the concept of energy balance in the field of earthquake engineering. The energy-based seismic design method combines two most important design parameters of force

and displacement. It can reveal the nature of seismic response from the perspective of energy dissipation, and it can more fully reflect the impact on structures and the seismic capacity of structures under earthquake excitation [13–16]. At present, the energy-based approach has been proved to be effective and helpful to determine the seismic design of a structure under long-period earthquake excitation [17–21]. To reasonably evaluate the seismic energy response, it is necessary to define some relevant parameters from the energy balance, such as input energy, hysteretic energy, damping energy, the ratio of hysteretic energy to input energy, the ratio of damping energy to input energy, et al. The energy response spectra corresponding to these parameters can effectively be applied in the research on the seismic energy response of a structure under earthquake excitation.

A lot of work has been accumulated on the seismic input energy of a structure under long-period ground motions. The resonance effects between long-period ground motions and high-rise buildings can be produced easily. As a result, the seismic input energy is expected to be several times higher than that in the seismic design [22]. Chen et al. [23] thought that the seismic input energy of TOM wave is mainly distributed from 4 s to 10 s, and it is so easy to cause resonance effect on the prototype structures whose vibration period is about 9 s. To this end, the seismic energy response to the long-period structures under long-period ground motions has attracted great attention in academia. However, it is not comprehensive about the types of energy response spectra and influential factors, such as source nature, earthquake magnitude, source-to-site distance, propagation path, site condition, and the site effect of long-period seismic events [1, 24, 25]. In addition, the vibration period and damping ratio are two key factors influencing the dynamic behavior of long-period structures [26–29]. So, it is necessary to study the influence on seismic energy response affected by the dynamic characteristic of a structure itself.

Two types of ground motions in the existing earthquake records are considered as special long-period ground motions; besides one is near-fault pulse-like ground motions, and the other is far-field harmonic ground motions. This paper aims to investigate the seismic energy response of SDOF systems under near-fault pulse-like and far-field harmonic ground motions. As we all know, the improved pulse classification algorithm proposed by Shahi and Baker is frequently used to classify up to five potential pulses for each ground motion [30], and the selected ground motions in this paper are rotated in line with the orientation of the strongest potential pulse. Taking reliable long-period earthquake records as the research object, the elastoplastic dynamic analysis program is employed to study the seismic energy response of SDOF systems under two types of typical long-period ground motions. The main parameters are total input energy (E_I), cumulative hysteretic energy dissipation (E_H), damping energy dissipation (E_D), the ratio of hysteretic energy to input energy (λ_H), and the ratio of damping energy to input energy (λ_D). Then, the external and internal factors affecting the energy response spectra and energy distribution rule are analyzed one by one. It can provide an important reference for the energy-based seismic design of long-period structures subjected to long-period ground motions.

2. Energy Equation and Energy Principle

The dynamic equilibrium equation for elastoplastic SDOF systems under earthquake excitation is

$$m\ddot{x}(t) + c\dot{x}(t) + f(x(t)) = -m\ddot{x}_g(t), \tag{1}$$

where m is the mass of SDOF systems; c is the viscous damping coefficient; $f(x(t))$ is the restoring force; $\ddot{x}(t)$, $\dot{x}(t)$, and $x(t)$ are the acceleration, velocity, and displacement response relative to the ground, respectively; and $\ddot{x}_g(t)$ is the ground acceleration at the moment of t.

The energy equation defined by the relative displacement of x can be obtained and rewritten as follows:

$$\int_0^x m\ddot{x}(t)\mathrm{d}x + \int_0^x c\dot{x}(t)\mathrm{d}x + \int_0^x f(x(t))\mathrm{d}x = -\int_0^x m\ddot{x}_{\mathrm{g}}(t)\mathrm{d}x. \tag{2}$$

The above energy equation can be rewritten as the following equation by substituting $\mathrm{d}x = \dot{x}\mathrm{d}t$:

$$\int_0^t m\ddot{x}(t)\dot{x}(t)\mathrm{d}t + \int_0^t c(\dot{x}(t))^2\mathrm{d}t + \int_0^t f(x(t))\dot{x}(t)\mathrm{d}t = -\int_0^t m\ddot{x}_{\mathrm{g}}(t)\dot{x}(t)\mathrm{d}t, \tag{3}$$

where $E_K(t) = \int_0^t m\ddot{x}(t)\dot{x}(t)\mathrm{d}t$ is the kinetic energy; $E_D(t) = \int_0^t c(\dot{x}(t))^2\mathrm{d}t$ is the damping energy dissipation; $E_S(t) + E_H(t) = \int_0^t f(x(t))\dot{x}(t)\mathrm{d}t$ is the elastic-strain energy dissipation and hysteretic energy dissipation; and $E_I(t) = -\int_0^t m\ddot{x}_{\mathrm{g}}(t)\dot{x}(t)\mathrm{d}t$ is the total input energy.

The above energy equation can be rewritten as follows:

$$E_K(t) + E_D(t) + E_S(t) + E_H(t) = E_I(t). \tag{4}$$

For elastoplastic SDOF systems, the energy dissipation capacity of a structure mainly depends on the cumulative hysteretic energy of E_H and damping energy of E_D, and the hysteretic energy of E_H accounts for a larger proportion. Therefore, the seismic design method based on the energy concept is to solve the cumulative hysteretic energy dissipation of E_H in equation (4). And then, more details about the load-bearing capacity and plastic deformation capacity of a structure could be understood further. Combining relevant literatures [31, 32], the ratio of hysteretic energy to input energy (RHEIE) can be defined as the ratio of structural cumulative hysteretic energy dissipation to the total input energy of a structure ($\lambda_H = E_H/E_I$), while the ratio of damping energy to input energy (RDEIE) can be defined as the ratio of structural damping energy dissipation to the total input energy of a structure ($\lambda_D = E_D/E_I$). These two important parameters can be employed to reasonably evaluate the energy distribution rule of a structure under earthquake excitation.

3. Energy Response Spectra of SDOF Systems under Long-Period Earthquake Records

3.1. Selection of Long-Period Earthquake Records. Common ground motions refer to the particular ground motions where the Fourier amplitude is evenly distributed over a wide-frequency range. "Long-period ground motions" refers to the particular ground motions where the Fourier amplitude is concentrated in a narrow low-frequency domain. In this study, a lot of effective and reliable near-fault pulse-like and far-field harmonic ground motions are selected as the record databases of long-period earthquake records. The multiple earthquake damage indicates that the long-period ground motions have an amplification effect on the dynamic response of long-period structures, and they easily cause resonance-like action and serious damage to long-period structures. Therefore, it is necessary to compare the seismic energy response of long-period structures subjected to long-period and common ground motions. Tables 1–3 show more detailed information about near-fault pulse-like, far-field harmonic and common ground motion records, respectively. The particular distance from the fault rupture surface for near-fault pulse-like earthquake is within 20 km, and it includes obvious fling-step and rupture-directivity effects. The particular distance from site soil to source for far-field harmonic earthquake is beyond 200 km, and its spectrum characteristics mainly rely on the site conditions of observation station and the selection effects of site soil.

However, earthquake records obtained from seismic stations contain both ground vibration information purely caused by an earthquake and much complex interference. The long-period components of these interferences drift the baseline of earthquake time-history curve. To remove the effect of nonseismic factors, it is necessary to correct the baseline of earthquake time-history before it is used for a further study. The polynomial linear type is employed to adjust the baseline, and the high-pass filtering Butterworth type is used to correct the existed baseline drifting. The low-frequency components are considered as much as possible to be retained during the filtering correction process. In the Fourier amplitude spectrum analysis, the frequency range of 0-1 Hz is considered to be a low-frequency band. If the Fourier amplitude of ground motions is mainly concentrated in the low-frequency band and it is also satisfied for the judgment condition of equation (5), this particular ground motion is thought to be special long-period ground motions.

$$\beta = \frac{\int_0^1 f(x)\mathrm{d}x}{\int_0^f f(x)\mathrm{d}x} \geq 0.8, \tag{5}$$

where $f(x)$ is the function of Fourier amplitude spectrum and f is the cut-off frequency, and the value of f is 20 Hz in this paper.

Figure 1(a) illustrates the corrected acceleration time histories. Figure 1(b) displays the corresponding Fourier amplitude spectrum of partial ground motions listed in Tables 1–3 in a visual informative manner. The frequency distribution of long-period ground motions is concentrated in a relatively low-frequency (0.1~1.0 Hz) band, and common ground motions are concentrated in a relatively high-frequency (1.0~2.3 Hz) band.

3.2. Calculation of Various Energy Response Spectra. According to the above energy equation and energy principle, various energy response spectra on the total input energy, hysteretic energy dissipation, and damping energy dissipation are calculated, respectively. The damping ratio of 5%, the ductility coefficient of 3.0, and the yield stiffness ratio of 0.05 are initially assumed based on the bilinear restoring force model of SDOF systems.

Figure 2 shows the average energy response spectra of SDOF systems under three types of ground motions. The energy response spectra on input energy, hysteretic energy, and damping energy under three types of ground motions have experienced obvious three-stage process. All the energy response spectra increase in the short period. After passing through a peak in the medium-long period, they begin to decrease. And they have no obvious change in the long period. Within the whole period, all the energy response spectra under near-fault pulse-like and far-field harmonic ground motions are greater than those under common ground motions, and the peak values of input energy spectra under near-fault pulse-like and far-field harmonic ground motions are 4.8 times and 32.3 times of those under common ground motions, respectively. For near-fault pulse-like ground motions, all the energy response spectra slowly increase before 4 s, while they gradually decrease from 4 s to 10 s. And they tend to be stable when the vibration period of SDOF systems is beyond 10 s. For far-field harmonic ground motions, all the energy response spectra quickly increase before 3 s, while they rapidly decrease after reaching at the peak. And then they tend to be stable. The energy response spectra under far-field harmonic ground motions are greater than those under near-fault pulse-like ground motions within the whole period.

4. Seismic Energy Response Affected by External Factors

External and internal factors are the two main factors affecting the seismic energy response of SDOF systems. External factors mainly refer to the characteristics of earthquake excitation, while internal factors mainly refer to the dynamic characteristics of a structure itself. Since the earthquake record is a nonstationary random time-series with a wide-frequency band, the characteristics of earthquake excitation mainly include the nature of source, the earthquake magnitude, the source-to-site distance, the spreading path, and the site condition. The seismic energy response of elastoplastic SDOF systems that are studied is affected by the external factors of earthquake magnitude and site condition.

Table 1: Basic information of near-fault pulse-like earthquake records.

No.	Earthquake events	Station component	M (M_w)	D (km)	S
1	Northridge	1085_SCE018	6.7	5.2	C
2	Northridge	1085_SCE288	6.7	5.2	C
3	Northridge	1084_SCS052	6.7	5.3	D
4	Northridge	1084_SCS142	6.7	5.3	D
5	Northridge	1086_SYL090	6.7	5.3	C
6	Northridge	1086_SYL360	6.7	5.3	C
7	Northridge	1045_WPI046	6.7	5.5	D
8	Northridge	1045_WPI316	6.7	5.5	D
9	Northridge	1013_LDM064	6.7	5.9	C
10	Northridge	1013_LDM334	6.7	5.9	C
11	Northridge	1044_NWH090	6.7	5.9	D
12	Northridge	1044_NWH360	6.7	5.9	D
13	Northridge	1063_RRS228	6.7	6.5	D
14	Northridge	1063_RRS318	6.7	6.5	D
15	Northridge	1050_PAC175	6.7	7	A
16	Northridge	1050_PAC265	6.7	7	A
17	Northridge	1052_PKC090	6.7	7.6	C
18	Northridge	1052_PKC360	6.7	7.6	C
19	Northridge	949_ARL090	6.7	8.7	D
20	Northridge	949_ARL360	6.7	8.7	D
21	Northridge	1082_RO3000	6.7	10.1	D
22	Northridge	1082_RO3090	6.7	10.1	D
23	Northridge	960_LOS000	6.7	12.4	D
24	Northridge	960_LOS270	6.7	12.4	D
25	Northridge	1083_GLE170	6.7	13.3	C
26	Northridge	1083_GLE260	6.7	13.3	C
27	Northridge	1080_KAT000	6.7	13.4	C
28	Northridge	1080_KAT090	6.7	13.4	C
29	Northridge	1087_TAR090	6.7	15.6	D
30	Northridge	1087_TAR360	6.7	15.6	D
31	Northridge	953_MUL009	6.7	17.1	D
32	Northridge	953_MUL279	6.7	17.1	D
33	Northridge	1016_NYA090	6.7	18.5	C
34	Northridge	1016_NYA180	6.7	18.5	C
35	Northridge	1012_LA0000	6.7	19.1	C
36	Northridge	1012_LA0090	6.7	19.1	C
37	Chichi	TCU068-EW	7.6	0.32	C
38	Chichi	TCU068-NS	7.6	0.32	C
39	Chichi	TCU065-EW	7.6	0.57	D
40	Chichi	TCU065-NS	7.6	0.57	D
41	Chichi	TCU052-EW	7.6	0.66	C
42	Chichi	TCU052-NS	7.6	0.66	C
43	Chichi	TCU102-EW	7.6	1.49	C
44	Chichi	TCU102-NS	7.6	1.49	C
45	Chichi	CHY080-EW	7.6	2.69	C
46	Chichi	CHY080-NS	7.6	2.69	C
47	Chichi	TCU103-EW	7.6	6.08	C
48	Chichi	TCU087-NS	7.6	6.98	C
49	Chichi	TCU120-EW	7.6	7.4	C
50	Chichi	TCU136-EW	7.6	8.27	C
51	Chichi	TCU136-NS	7.6	8.27	C
52	Chichi	CHY006-EW	7.6	9.76	C
53	Chichi	CHY006-NS	7.6	9.76	C
54	Chichi	TCU138-NS	7.6	9.78	C
55	Chichi	TCU063-EW	7.6	9.78	C
56	Chichi	TCU063-NS	7.6	9.78	C
57	Chichi	CHY029-EW	7.6	10.96	C
58	Chichi	CHY029-NS	7.6	10.96	C
59	Chichi	TCU100-NS	7.6	11.37	C
60	Chichi	TCU116-EW	7.6	12.38	C

Table 1: Continued.

No.	Earthquake events	Station component	M (M_w)	D (km)	S
61	Chichi	TCU116-NS	7.6	12.38	C
62	Chichi	CHY035-EW	7.6	12.65	C
63	Chichi	CHY035-NS	7.6	12.65	C
64	Chichi	TCU104-EW	7.6	12.87	C
65	Chichi	TCU104-NS	7.6	12.87	C
66	Chichi	TCU109-EW	7.6	13.06	C
67	Chichi	TCU109-NS	7.6	13.06	C
68	Chichi	TCU128-EW	7.6	13.13	C
69	Chichi	TCU128-NS	7.6	13.13	C
70	Chichi	TCU074-EW	7.6	13.46	C
71	Chichi	TCU074-NS	7.6	13.46	C
72	Chichi	TCU048-EW	7.6	13.53	C
73	Chichi	TCU048-NS	7.6	13.53	C
74	Chichi	CHY034-EW	7.6	14.82	C
75	Chichi	CHY034-NS	7.6	14.82	C
76	Chichi	TCU123-EW	7.6	14.91	D
77	Chichi	TCU123-NS	7.6	14.91	D
78	Chichi	TCU107-EW	7.6	15.99	C
79	Chichi	TCU107-NS	7.6	15.99	C
80	Chichi	TCU064-EW	7.6	16.59	C
81	Chichi	TCU064-NS	7.6	16.59	C
82	Chichi	CHY104-EW	7.6	18.02	D
83	Chichi	CHY104-NS	7.6	18.02	D
84	Chichi	CHY025-EW	7.6	19.07	D
85	Chichi	CHY025-NS	7.6	19.07	D
86	Chichi	TCU036-EW	7.6	19.83	C
87	Chichi	TCU036-NS	7.6	19.83	C
88	Chichi	TCU039-EW	7.6	19.89	C
89	Chichi	TCU039-NS	7.6	19.89	C

4.1. Energy Response Spectra Affected by the Characteristic of Earthquake Excitation

4.1.1. Earthquake Magnitude. Taken as an example are the ground motions in the site class C of near-fault pulse-like earthquake records (listed in Table 1), and the selected earthquake records are classified as M_W 6.7 and M_W 7.6. Taken as an example are the ground motions in the site class D of far-field harmonic earthquake records, and the selected earthquake records are classified as M_W 7.3, M_W 8.0, and M_W 9.0. Various energy response spectra on the total input energy, hysteretic energy dissipation, and damping energy dissipation are calculated out under near-fault pulse-like and far-field harmonic ground motions, respectively. The damping ratio of 5%, the ductility coefficient of 3.0, and the yield stiffness ratio of 0.05 are initially assumed based on the bilinear restoring force model of SDOF systems.

The numbers of samples in each earthquake magnitude of near-fault pulse-like and far-field harmonic ground motion records are exhibited in Figure 3. Figures 4 and 5 illustrate the influence of earthquake magnitude on various energy response spectra under near-fault pulse-like and far-field harmonic ground motions. The peaks of various energy response spectra under two types of long-period ground motions show a rising trend with the increase of earthquake magnitude. Because the earthquake magnitude can roughly represent the characteristic of source mechanism and reflect the energy scale induced by earthquake excitation. The larger the earthquake magnitude, the greater the energy scale induced by earthquake excitation. The input energy grows with the increase of earthquake magnitude, which results in the rising hysteretic energy and damping energy. As the earthquake magnitude increases, the peaks of various energy response spectra under near-fault pulse-like ground motions rise more significantly than those under far-field harmonic ground motions. For example, the peak values on input energy, hysteretic energy, and damping energy at M_W 7.6 are 7.7, 8.6, and 7.1 times of those at M_W 6.7 under near-fault pulse-like ground motions respectively. For far-field harmonic ground motions, the input energy, hysteretic energy, and damping energy have little change with the increase of earthquake magnitude in the short period of 0–2 s. They increase gradually with the increase of earthquake magnitude in the medium-long period of 2–8 s. When the vibration period of SDOF systems is beyond 8 s, the input energy and hysteretic energy reduce gradually, but the damping energy basically remains unchanged with the increase of earthquake magnitude.

4.1.2. Site Condition. Taken as an example are ground motions in M_W 6.7 of near-fault pulse-like earthquake records, and the selected earthquake records are classified as the site class C and D. Taken as an example are ground motions in M_W 8.0 of far-field harmonic ground motions, and the selected earthquake records are classified as the site

Table 2: Basic information of far-field harmonic earthquake records.

No.	Earthquake events	Station component	M (M_w)	D (km)	S
1	Kumamoto	EHMH07-EW2	7.3	203	D
2	Kumamoto	EHMH07-NS2	7.3	203	D
3	Kumamoto	EHM016-EW	7.3	213	D
4	Kumamoto	EHM016-NS	7.3	213	D
5	Kumamoto	SMNH09-EW2	7.3	233	C
6	Kumamoto	SMNH09-NS2	7.3	233	C
7	Kumamoto	EHMH04-EW2	7.3	249	D
8	Kumamoto	EHMH04-NS2	7.3	249	D
9	Kumamoto	HRS004-EW	7.3	260	C
10	Kumamoto	HRS004-NS	7.3	260	C
11	Kumamoto	KOCH13-EW2	7.3	285	C
12	Kumamoto	KOCH13-NS2	7.3	285	C
13	Kumamoto	OKYH06-EW2	7.3	333	C
14	Kumamoto	OKYH06-NS2	7.3	333	C
15	Kumamoto	TKS005-EW	7.3	360	D
16	Kumamoto	TKS005-NS	7.3	360	D
17	Kumamoto	TTR006-EW	7.3	404	D
18	Kumamoto	TTR006-NS	7.3	404	D
19	Kumamoto	OSK010-EW	7.3	454	D
20	Kumamoto	OSK010-NS	7.3	454	D
21	Kumamoto	NAR007-EW	7.3	490	C
22	Kumamoto	NAR007-NS	7.3	490	C
23	Kumamoto	KYTH04-EW2	7.3	523	B
24	Kumamoto	KYTH04-NS2	7.3	523	B
25	Kumamoto	MIEH03-EW2	7.3	557	C
26	Kumamoto	MIEH03-NS2	7.3	557	C
27	Kumamoto	MIEH07-EW2	7.3	587	C
28	Kumamoto	MIEH07-NS2	7.3	587	C
29	Kumamoto	AIC001-EW	7.3	620	E
30	Kumamoto	AIC001-NS	7.3	620	E
31	Kumamoto	AIC015-EW	7.3	654	D
32	Kumamoto	AIC015-NS	7.3	654	D
33	Kumamoto	GIFH24-EW2	7.3	683	B
34	Kumamoto	GIFH24-NS2	7.3	683	B
35	Kumamoto	NGN024-EW	7.3	721	D
36	Kumamoto	NGN024-NS	7.3	721	D
37	Tokachi	IUBH03-EW	8.0	206	E
38	Tokachi	IUBH03-NS	8.0	206	E
39	Tokachi	HKD130-EW	8.0	241	C
40	Tokachi	HKD130-NS	8.0	241	C
41	Tokachi	ABSH04-EW2	8.0	280	C
42	Tokachi	ABSH04-NS2	8.0	280	C
43	Tokachi	HKD151-EW	8.0	318	D
44	Tokachi	HKD151-NS	8.0	318	D
45	Tokachi	AOM018-EW	8.0	343	C
46	Tokachi	AOM018-NS	8.0	343	C
47	Tokachi	HKD025-EW	8.0	374	D
48	Tokachi	HKD025-NS	8.0	374	D
49	Tokachi	AKT013-EW	8.0	399	C
50	Tokachi	AKT013-NS	8.0	399	C
51	Tokachi	AKT018-EW	8.0	437	D
52	Tokachi	AKT018-NS	8.0	437	D
53	Tokachi	YMT001-EW	8.0	482	E
54	Tokachi	YMT001-NS	8.0	482	E
55	Tokachi	YMTH14-EW2	8.0	513	D
56	Tokachi	YMTH14-NS2	8.0	513	D
57	Tokachi	YMT015-EW	8.0	548	E
58	Tokachi	YMT015-NS	8.0	548	E
59	Tokachi	FKS020-EW	8.0	580	E
60	Tokachi	FKS020-NS	8.0	580	E

Table 2: Continued.

No.	Earthquake events	Station component	M (M_w)	D (km)	S
61	Tokachi	FKSH21-EW2	8.0	640	C
62	Tokachi	FKSH21-NS2	8.0	640	C
63	Tokachi	NIGH11-EW2	8.0	687	C
64	Tokachi	NIGH11-NS2	8.0	687	C
65	Tokachi	NGNH28-EW2	8.0	763	B
66	Tokachi	NGNH28-NS2	8.0	763	B
67	East Japan	MYG005-EW	9.0	208	D
68	East Japan	MYG005-NS	9.0	208	D
69	East Japan	YMT002-EW	9.0	236	D
70	East Japan	YMT002-NS	9.0	236	D
71	East Japan	YMTH12-EW2	9.0	256	C
72	East Japan	YMTH12-NS2	9.0	256	C
73	East Japan	FKSH03-EW2	9.0	279	D
74	East Japan	FKSH03-NS2	9.0	279	D
75	East Japan	NIG009-EW	9.0	310	E
76	East Japan	NIG009-NS	9.0	310	E
77	East Japan	AOMH10-EW2	9.0	336	D
78	East Japan	AOMH10-NS2	9.0	336	D
79	East Japan	AOM019-EW	9.0	366	E
80	East Japan	AOM019-NS	9.0	366	E
81	East Japan	CHBH20-EW2	9.0	416	A
82	East Japan	CHBH20-NS2	9.0	416	A
83	East Japan	NIGH17-EW2	9.0	443	C
84	East Japan	NIGH17-NS2	9.0	443	C
85	East Japan	YMN010-EW	9.0	472	C
86	East Japan	YMN010-NS	9.0	472	C
87	East Japan	YMNH13-EW2	9.0	500	B
88	East Japan	YMNH13-NS2	9.0	500	B
89	East Japan	HKD102-EW	9.0	531	D
90	East Japan	HKD102-NS	9.0	531	D
91	East Japan	SZOH53-EW2	9.0	562	B
92	East Japan	SZOH53-NS2	9.0	562	B
93	East Japan	AIC005-EW	9.0	599	D
94	East Japan	AIC005-NS	9.0	599	D
95	East Japan	AIC003-EW	9.0	636	E
96	East Japan	AIC003-NS	9.0	636	E
97	East Japan	HKD030-EW	9.0	676	D
98	East Japan	HKD030-NS	9.0	676	D
99	East Japan	ABSH01-EW2	9.0	714	B
100	East Japan	ABSH01-NS2	9.0	714	B

class C, D, and E. Various energy response spectra on the total input energy, hysteretic energy dissipation, and damping energy dissipation are calculated under near-fault pulse-like and far-field harmonic ground motions, respectively. The damping ratio of 5%, the ductility coefficient of 3.0, and the yield stiffness ratio of 0.05 are initially assumed based on the bilinear restoring force model of SDOF systems.

The numbers of samples in each site class of near-fault pulse-like and far-field harmonic ground motion records are exhibited in Figure 6. Figures 7 and 8 illustrate the influence of site class on various energy response spectra under near-fault pulse-like and far-field harmonic ground motions. The peaks of various energy response spectra under two types of long-period ground motions show a rising trend with the softer of site soil, and their increased amplifications even aggravate when the site soil softens. For near-fault pulse-like ground motions, the site condition has a great influence on various energy response spectra in the period range of 1–5 s. When the vibration period of SDOF systems is beyond 5 s, the site condition has little influence on the hysteretic energy and damping energy. For far-field harmonic ground motions, various energy response spectra are almost not affected by site condition in the short period of 0-1 s. They show a rising trend with the softer of site soil in the medium-long period of 1–10 s, and their increased amplifications are significant. When the vibration period of SDOF systems is beyond 10 s, their increased amplifications relatively get smaller.

4.2. Energy Distribution Rule Affected by the Characteristic of Earthquake Excitation. After obtaining the total input energy, hysteretic energy dissipation and damping energy dissipation, the ratio of hysteretic energy to input energy (RHEIE), and the ratio of damping energy to input energy

Table 3: Basic information of common earthquake records.

No.	Earthquake events	Station component	Magnitude (M_w)	Distance (km)	Site class
1	Imperial Valley	ELC000	5.0	34.98	D
2	Imperial Valley	ELC090	5.0	34.98	D
3	Imperial Valley	ELC180	6.59	6.09	D
4	Imperial Valley	ELC270	6.59	6.09	D
5	Kobe	OKA000	6.9	86.94	C
6	Kobe	OKA090	6.9	86.94	C
7	Tabas_ Iran	TAB-L1	7.35	2.05	B
8	Tabas_ Iran	TAB-T1	7.35	2.05	B
9	Kern County	TAF021	7.36	38.89	C
10	Kern County	TAF111	7.36	38.89	C
11	Kern County	PAS180	7.36	125.59	C
12	Kern County	PAS270	7.36	125.59	C
13	Kobe	OSA000	6.9	21.35	D
14	Kobe	OSA090	6.9	21.35	D
15	Kobe	SHI000	6.9	19.15	D
16	Kobe	SHI090	6.9	19.15	D
17	Loma Prieta	AGW000	6.93	24.57	D
18	Loma Prieta	AGW090	6.93	24.57	D
19	Loma Prieta	HCH090	6.93	27.6	D
20	Loma Prieta	HCH180	6.93	27.6	D
21	Superstition Hill (B)	B-ICC000	6.54	18.2	D
22	Superstition Hill (B)	B-ICC090	6.54	18.2	D
23	Superstition Hill (B)	B-WSM090	6.54	13.03	D
24	Superstition Hill (B)	B-WSM180	6.54	13.03	D
25	Superstition Hill (B)	B-IVW090	6.54	23.85	E
26	Superstition Hill (B)	B-IVW360	6.54	23.85	E

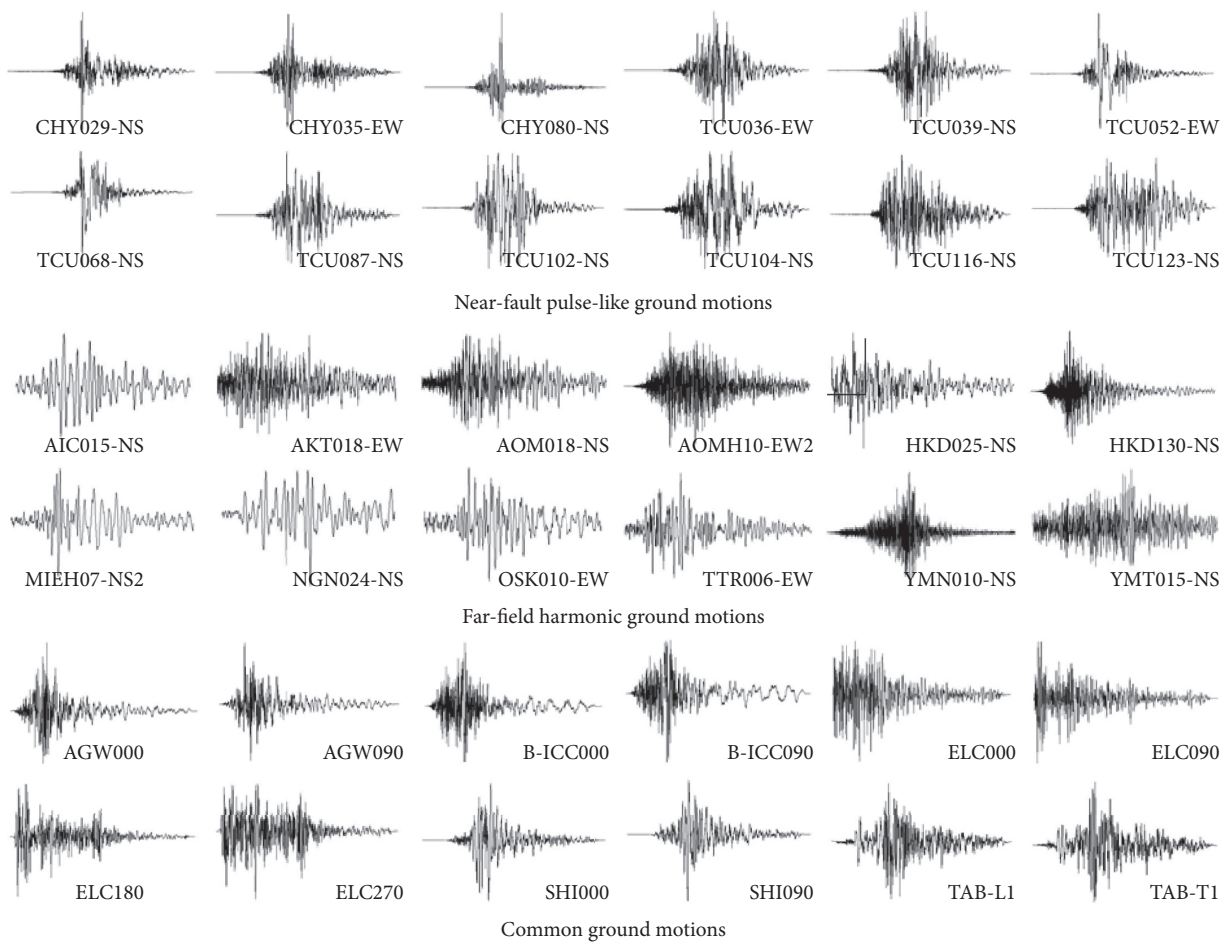

(a)

Figure 1: Continued.

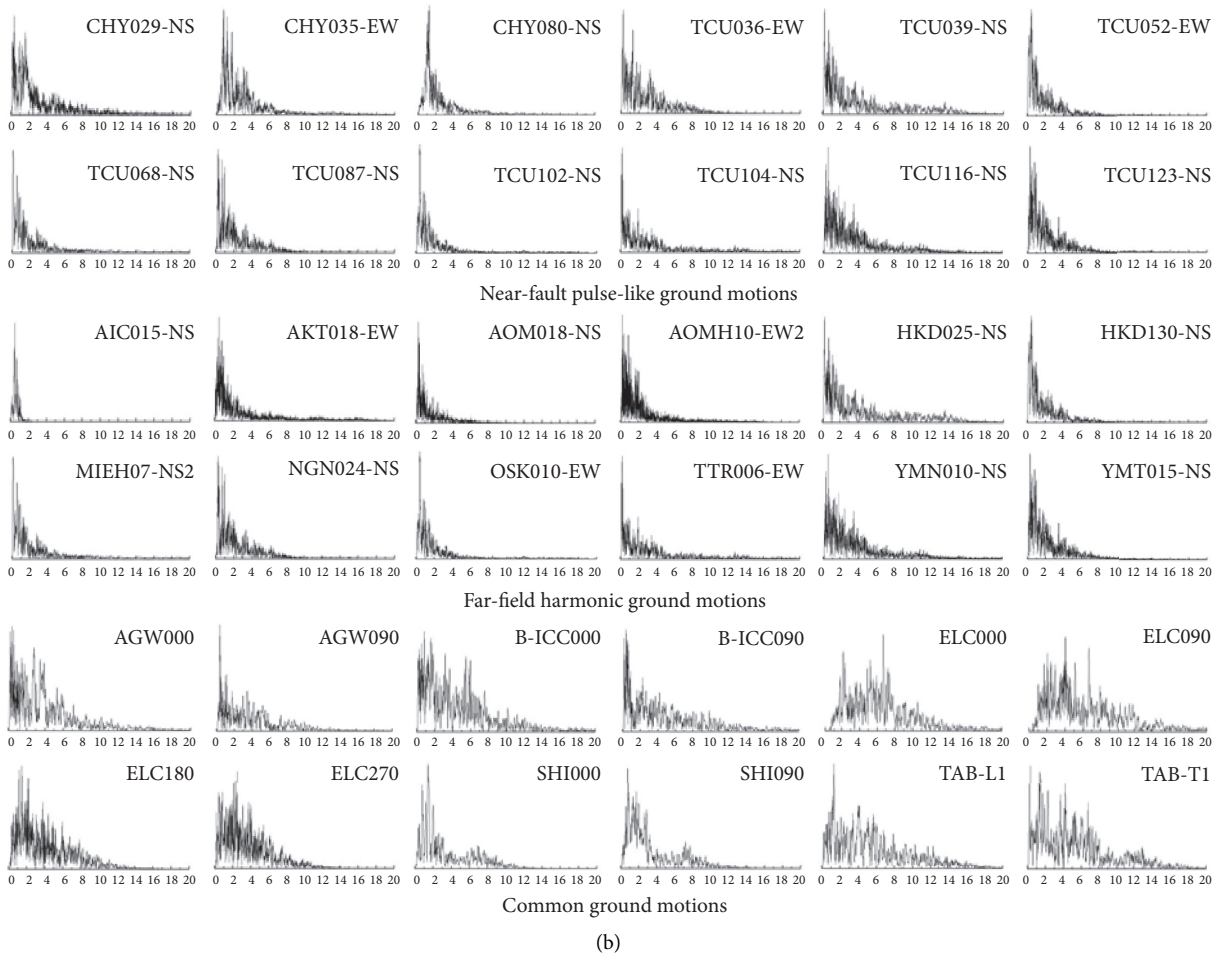

(b)

Figure 1: Basic property of partial earthquake records. (a) Acceleration time histories (s). (b) Fourier amplitude spectrum (Hz).

(RDEIE) of SDOF systems could be calculated out under earthquake excitation. The energy distribution rule of elastoplastic SDOF systems studied is affected by the external factors of earthquake magnitude and site condition under near-fault pulse-like and far-field harmonic ground motions, respectively.

4.2.1. Earthquake Magnitude. Figures 9 and 10 illustrate the influence of earthquake magnitude on the energy distribution rule of SDOF systems under two types of long-period ground motions. For near-fault pulse-like ground motions, the distribution rule on total input energy is hardly affected by earthquake magnitude in the short period of 0–2 s. The RHEIE and RDEIE both decrease in the medium and long period. Particularly when the earthquake magnitude is M_W 6.7, the decline of RHEIE and RDEIE reaches 62.5% and 40.4%. The total seismic input energy of a structure with medium or long vibration period mainly depends on the damping energy to dissipate. The low-magnitude near-fault pulse-like earthquake always induces less inelastic deformation, so it would mitigate the structural damage. For far-field harmonic ground motions, the decline of RHEIE reaches 33.6% at M_W 7.3. The RHEIE varies within 60%–68% at M_W 8.0 and M_W 9.0. The hysteretic energy is the main way to dissipate the total seismic input energy of a structure under large magnitude far-field harmonic earthquake. However, the large magnitude far-field harmonic earthquake would exacerbate the structural damage due to the increased inelastic deformation. The RDEIE slightly grows with the increase of earthquake magnitude, and it does not significantly change along the vibration period of SDOF systems.

4.2.2. Site Condition. Figures 11 and 12 illustrate the influence of site class on the energy distribution rule of SDOF systems under two types of long-period ground motions. For near-fault pulse-like ground motions, the RHEIE and RDEIE both decrease in the site class C and D and the decline of RHEIE reaches 40% or so. The RHEIE in the site class D is slightly larger than that in the site class C, but the RDEIE is hardly affected by site class. For far-field harmonic ground motions, the RHEIE decrease in the site class C, D, and E. Specifically speaking, the decline of RHEIE in the site class C and D is about 30.5% and 28.8%, respectively. However, the RHEIE in the site class E is greatly different from that in above two types of site class in the period of

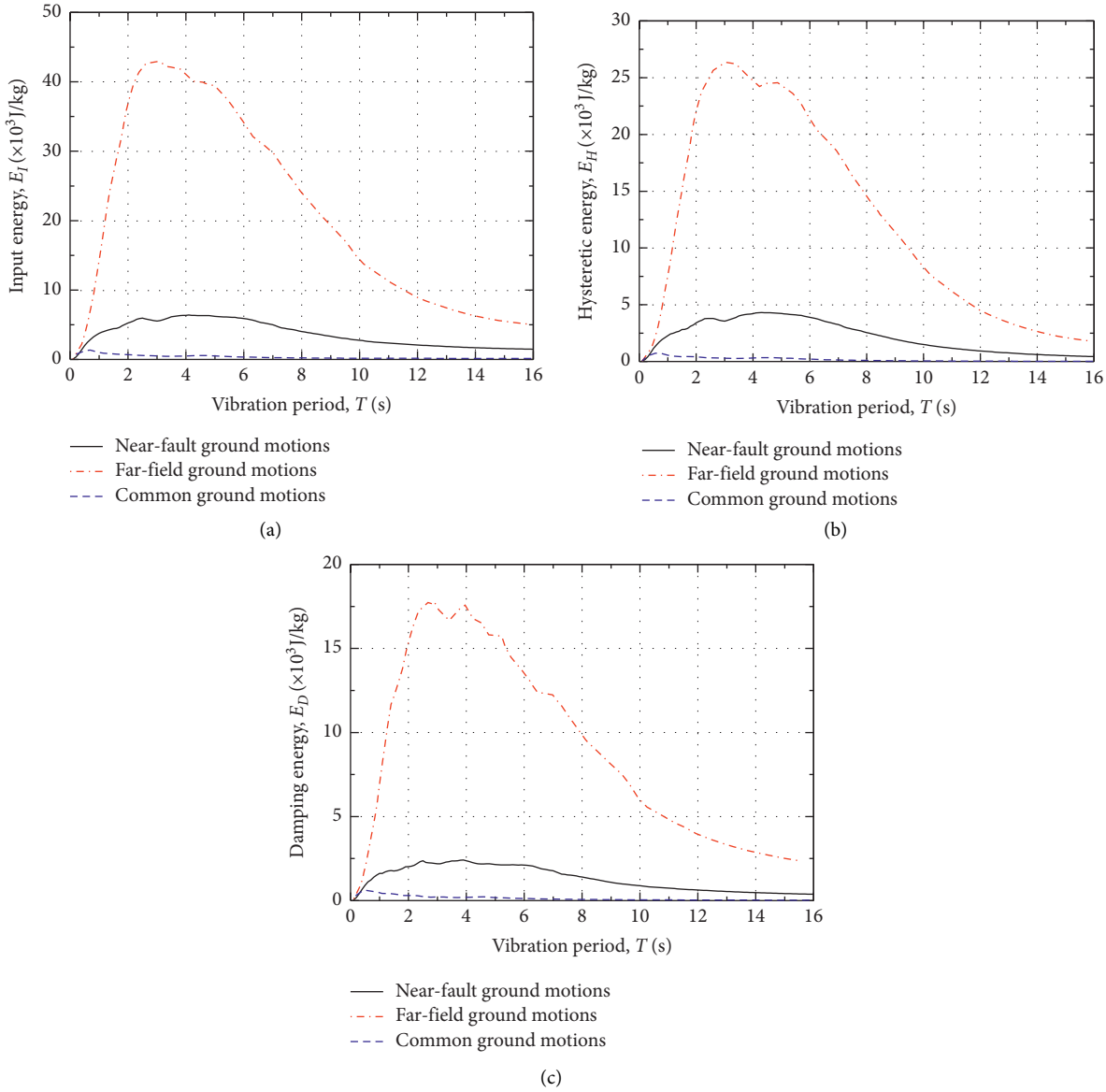

Figure 2: Energy response spectra. (a) Input energy. (b) Hysteretic energy. (c) Damping energy.

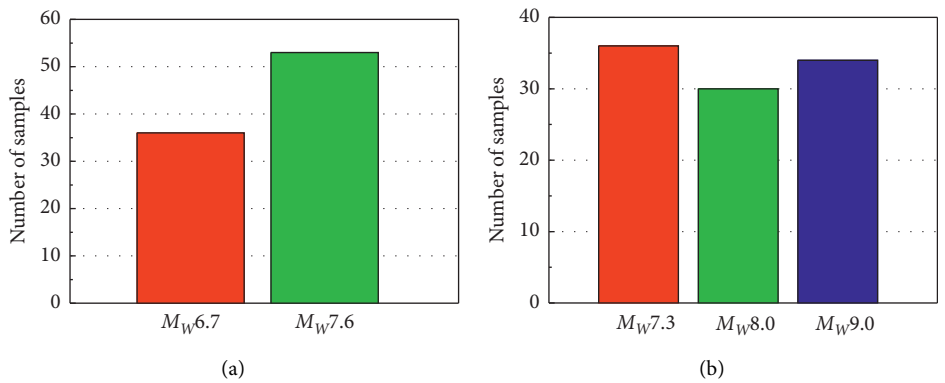

Figure 3: Numbers of samples in each earthquake magnitude. (a) Near-fault pulse-like ground motions. (b) Far-field harmonic ground motions.

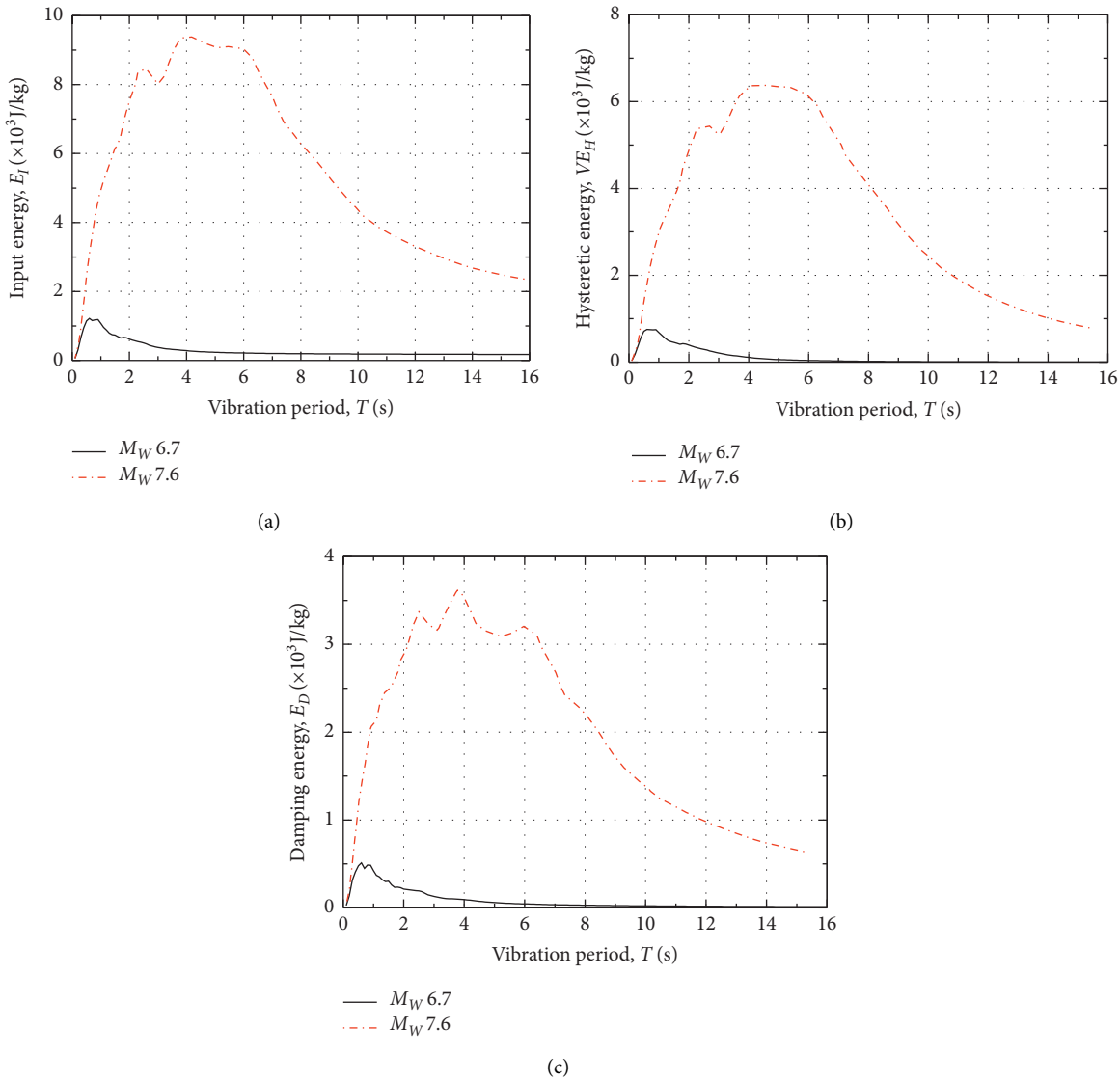

Figure 4: Energy response spectra affected by earthquake magnitude under near-fault pulse-like ground motions. (a) Input energy. (b) Hysteretic energy. (c) Damping energy.

5–16 s, even the maximum difference is up to 48.2%. The RDEIEs in the site class C, D, and E are within the fluctuation of 45%–55%.

5. Energy Response Spectra Affected by Internal Factors

Previous context has done much detailed analysis on the external factors. From the internal factors, the dynamic characteristic of a structure mainly include the damping model, the restoring force model, the damping ratio, the ductility coefficient, the second stiffness coefficient, and the yield displacement. The seismic energy response of elasto-plastic SDOF systems are studied affected by the internal factors of damping ratio, ductility coefficient, and yield stiffness ratio.

5.1. Input Energy Spectra Affected by the Dynamic Characteristic of a Structure

5.1.1. Damping ratio. The ductility coefficient of 3.0 and the damping ratio of 0.02, 0.05, 0.1, and 0.2 are initially assumed based on the bilinear restoring force model. Figure 13 shows the influence of damping ratio on the input energy spectra under near-fault pulse-like and far-field harmonic ground motions. As the ductility coefficient of 3.0 keeps constant, the peaks on input energy spectra about two types of long-period ground motions slowly drop with the increase of damping ratio. As the damping ratio increases, the input energy spectra drop on the left side of demarcation point, while the input energy spectra grow on the right side of demarcation point. Compared with near-fault pulse-like ground motions, the specific period corresponding to the peak of input energy spectra tends to the short-period

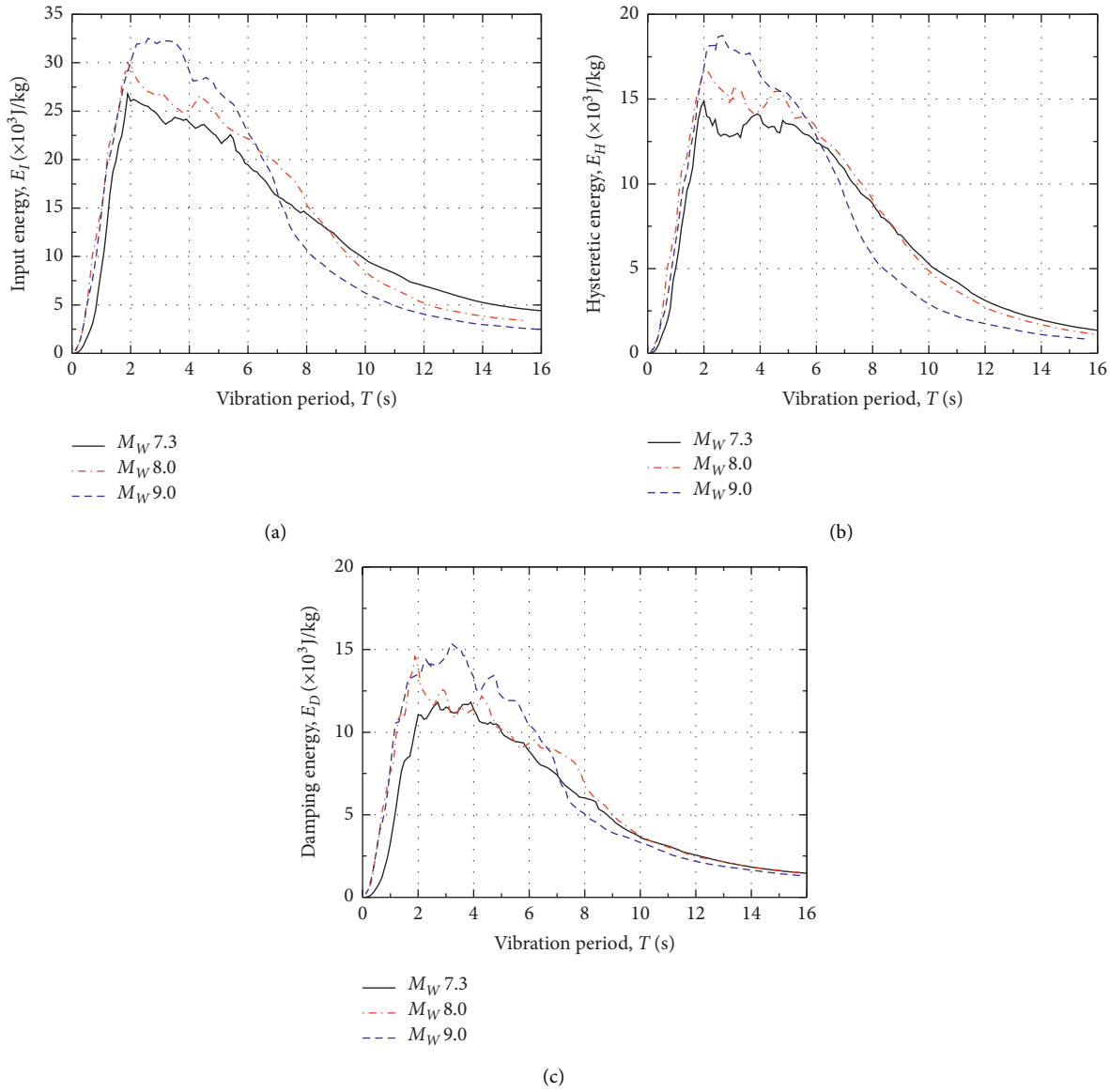

Figure 5: Energy response spectra affected by earthquake magnitude under far-field harmonic ground motions. (a) Input energy. (b) Hysteretic energy. (c) Damping energy.

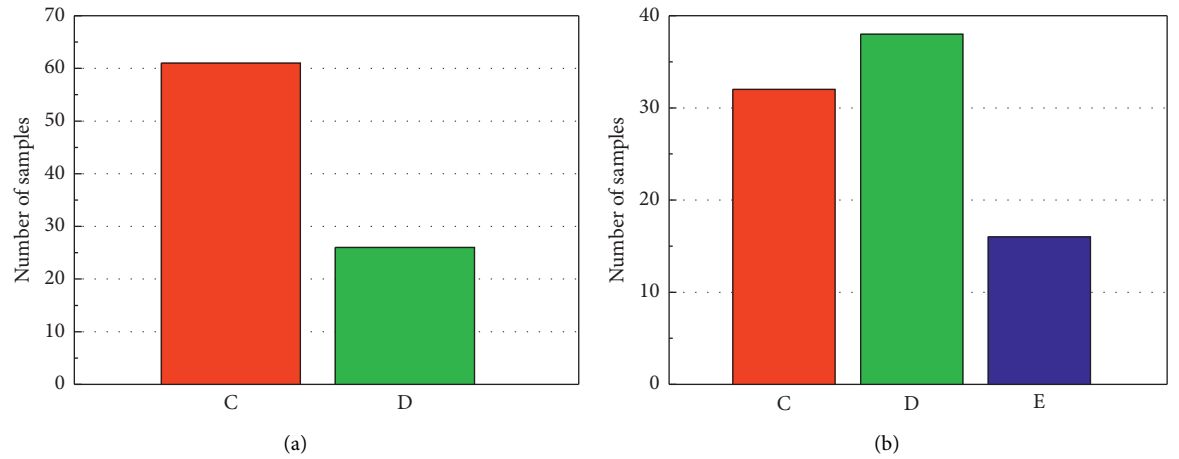

Figure 6: Numbers of samples in each site class. (a) Near-fault pulse-like ground motions. (b) Far-field harmonic ground motions.

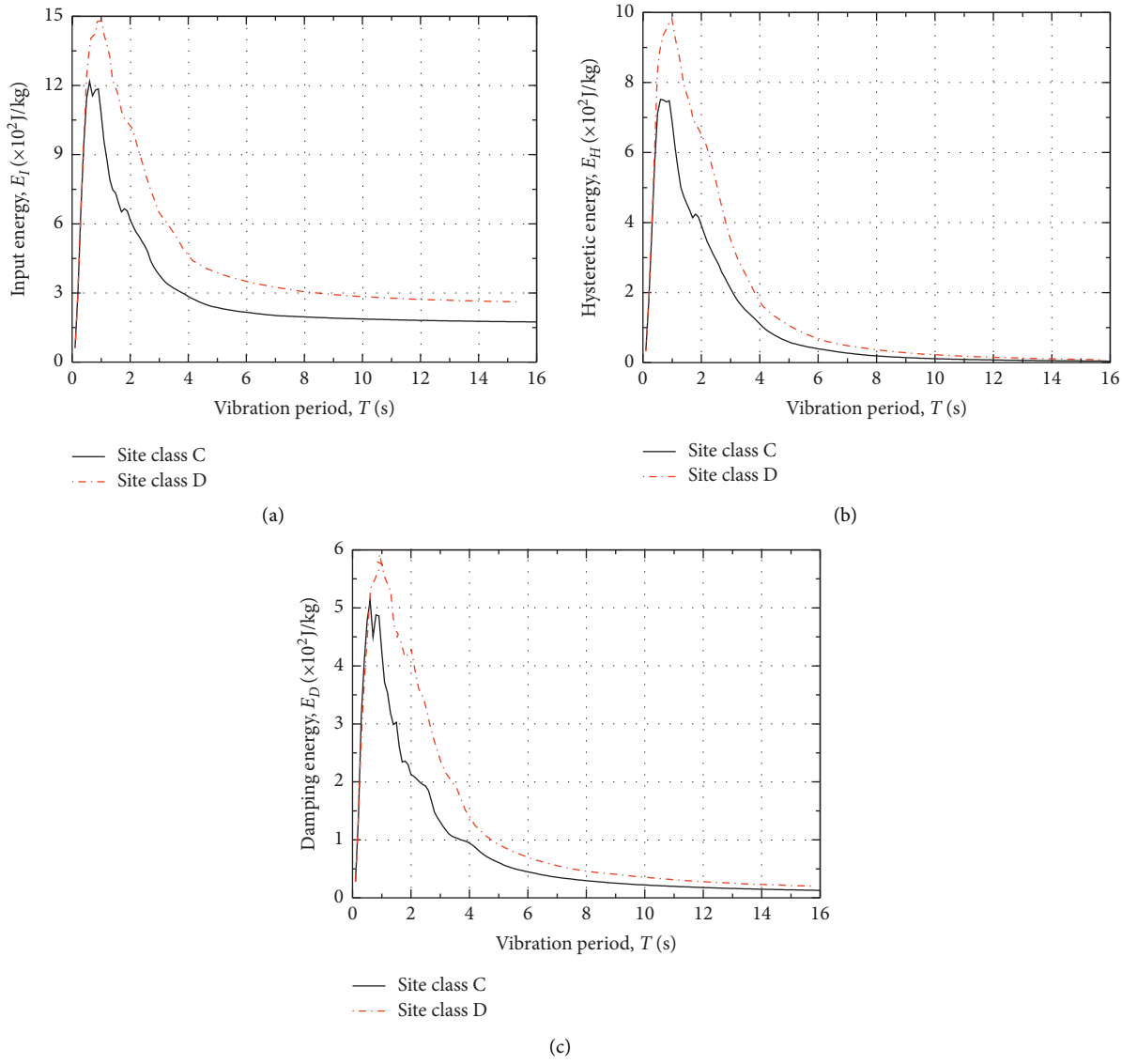

FIGURE 7: Energy response spectra affected by site class under near-fault pulse-like ground motions. (a) Input energy. (b) Hysteretic energy. (c) Damping energy.

direction under far-field harmonic ground motions. As the ductility coefficient of 3.0 keeps constant, the input energy spectra under two types of long-period ground motions are almost not affected by damping ratio in the short period of 0–2 s. The influence of damping ratio on the input energy spectra of near-fault pulse-like ground motions is greater than that of far-field harmonic ground motions in the medium–long period of 2–7 s. On the contrary, the influence of damping ratio on the input energy spectra of near-fault pulse-like ground motions is less than that of far-field harmonic ground motions when the vibration period is beyond 7 s.

5.1.2. Ductility Coefficient. The damping ratio of 5% and the ductility coefficient of 1, 3, 5, and 8 are initially assumed based on the bilinear restoring force model. Figure 14 shows the influence of ductility coefficient on the input energy spectra under near-fault pulse-like and far-field harmonic ground motions. As the damping ratio of 5% keeps constant, the peaks on input energy spectra about two types of long-period ground motions continuously drop with the increase of ductility coefficient. As the ductility coefficient increases, the specific period corresponding to the peak of input energy spectra tends to the short-period direction more significantly under near-fault pulse-like ground motions than that under far-field harmonic ground motions. For two types of long-period ground motions, the input energy spectra are almost the same under different ductility coefficient in the short period of 0–2.8 s. The input energy spectra show a decreasing trend with the increase of ductility coefficient in the period range of 2.8–12 s. The input energy spectra of two types of long-period ground motions tend to be stable when the vibration period is beyond 12 s.

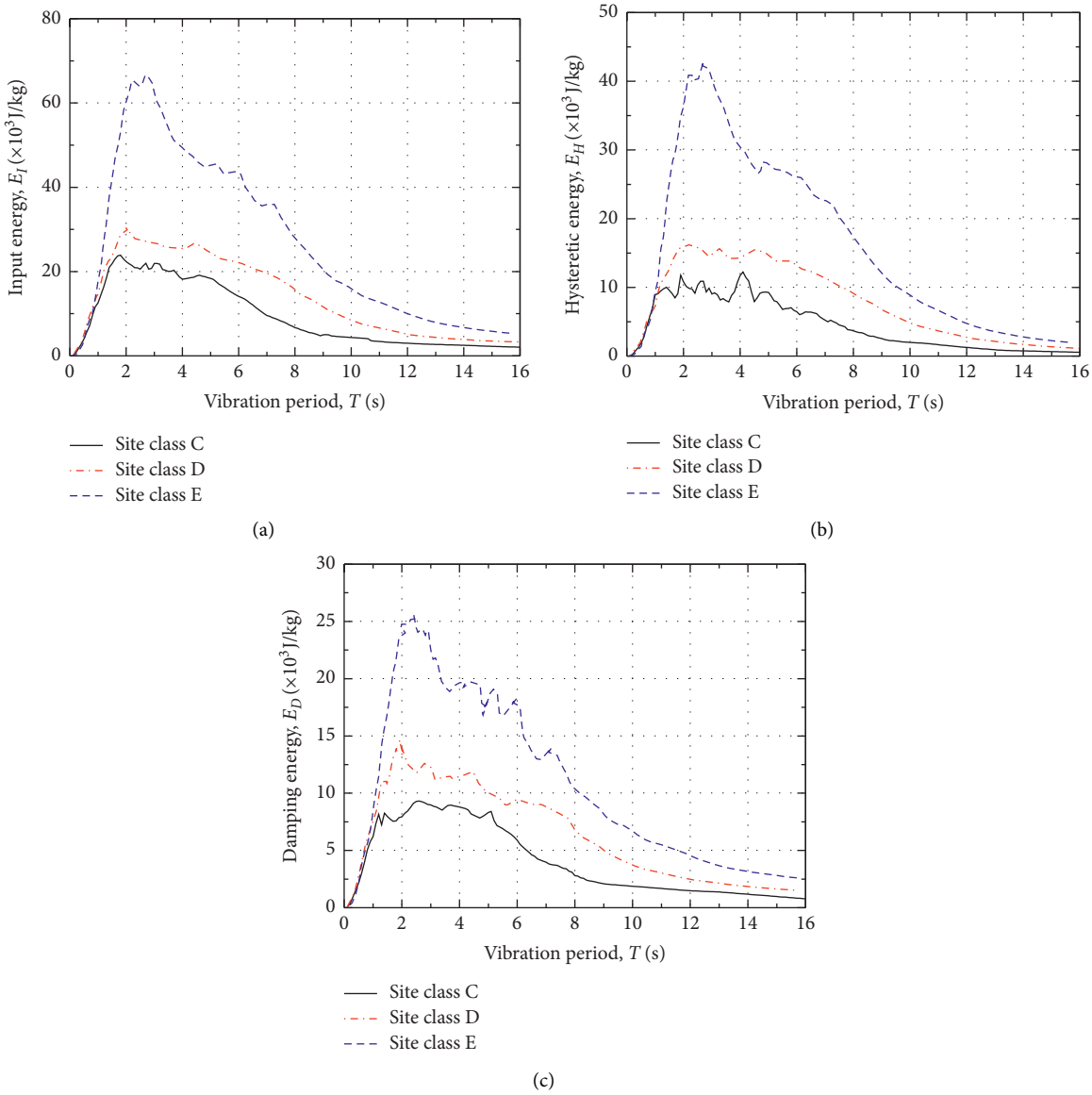

Figure 8: Energy response spectra affected by site class under far-field harmonic ground motions. (a) Input energy. (b) Hysteretic energy. (c) Damping energy.

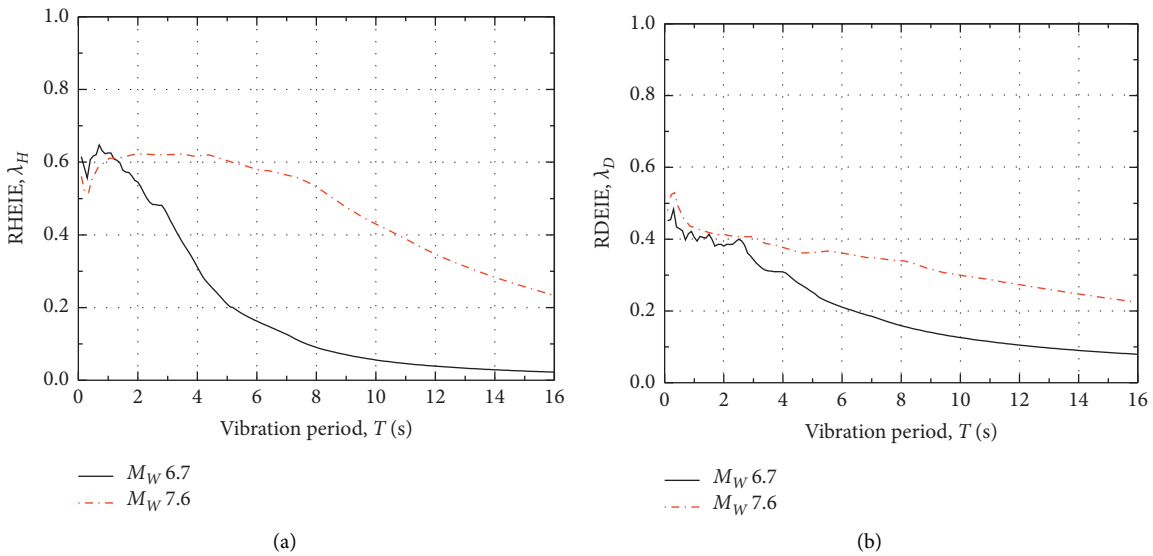

Figure 9: Energy distribution rule affected by earthquake magnitude under near-fault pulse-like ground motions. (a) RHEIE. (b) RDEIE.

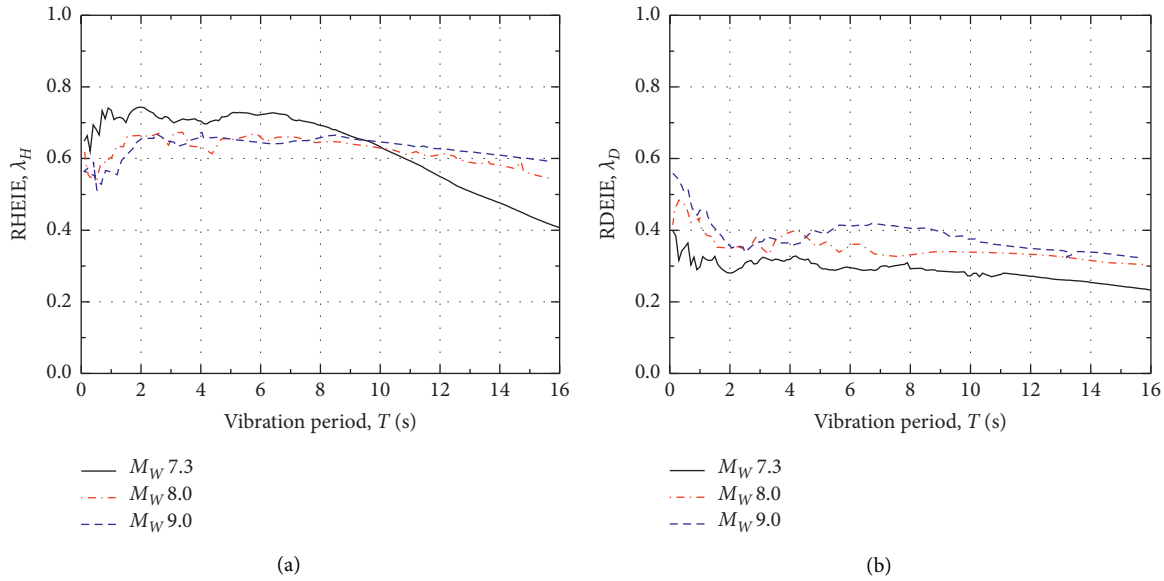

Figure 10: Energy distribution rule affected by earthquake magnitude under far-field harmonic ground motions. (a) RHEIE. (b) RDEIE.

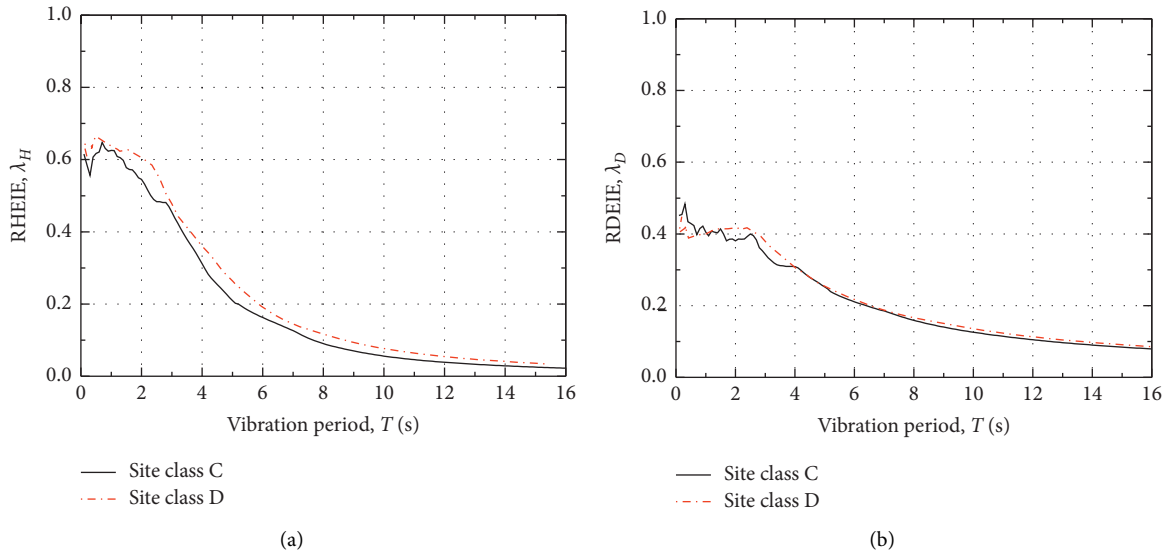

Figure 11: Energy distribution rule affected by site class under near-fault pulse-like ground motions. (a) RHEIE. (b) RDEIE.

5.2. *Hysteretic Energy Spectra Affected by the Dynamic Characteristic of a Structure*

5.2.1. Damping ratio. The ductility coefficient of 3.0 and the damping ratio of 0.02, 0.05, 0.1, and 0.2 are initially assumed based on the bilinear restoring force model. Figure 15 shows the influence of damping ratio on the hysteretic energy spectra under near-fault pulse-like and far-field harmonic ground motions. On the whole, the influence of damping ratio on the hysteretic energy spectra under two types of long-period ground motions is mainly reflected in the vicinity of the specific period corresponding to the peak. The influence of damping ratio on the hysteretic energy spectra is not significant in the short and long period. The peaks on hysteretic energy spectra under two types of long-period ground motions significantly drop with the increase of damping ratio. The specific period corresponding to the peak of hysteretic energy tends to the short-period direction under far-field harmonic ground motions. The hysteretic energy spectra under two types of long-period ground motions both reduce with the increase of damping ratio, and this property is manifested in the whole period range. It indicates that the damping ratio has a significant influence on the distribution rule of total input energy dissipation. The greater the damping ratio, the smaller the RHEIE (that is, the greater the RDEIE). Therefore, damping ratio plays an important role in the distribution rule of total input energy dissipation among the hysteretic energy and damping energy.

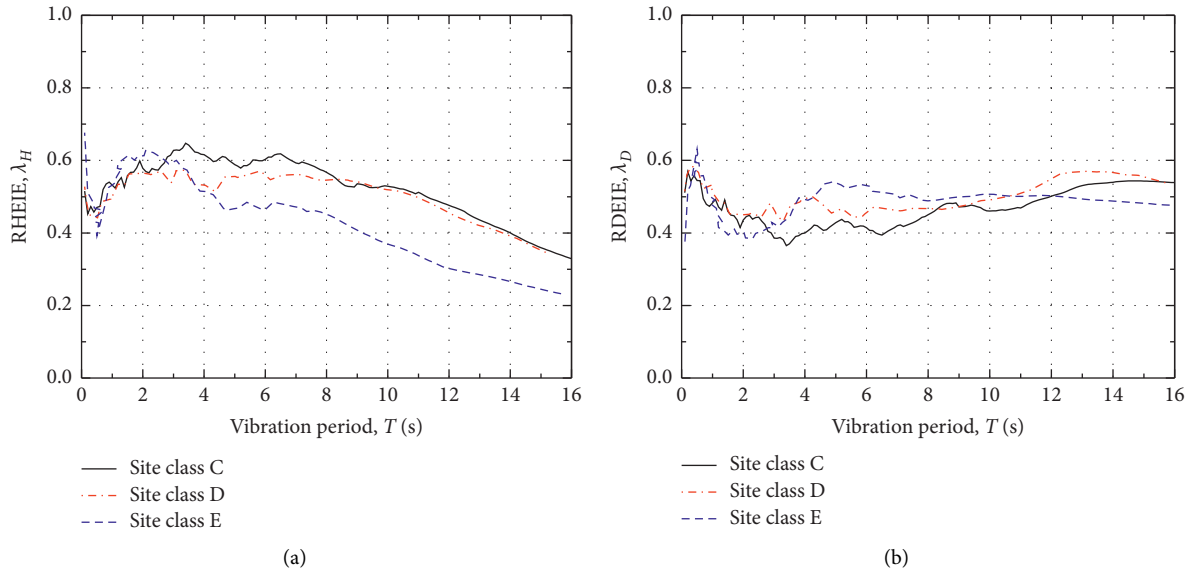

Figure 12: Energy distribution rule affected by site class under far-field harmonic ground motions. (a) (a) RHEIE. (b) RDEIE.

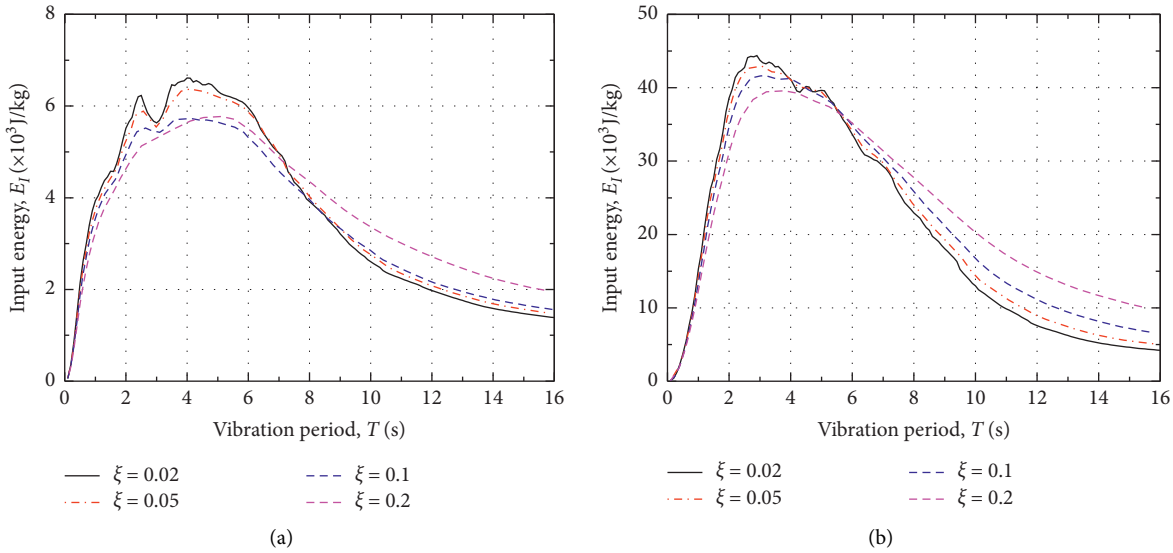

Figure 13: Input energy spectra affected by damping ratio. (a) Near-fault pulse-like ground motions. (b) Far-field harmonic ground motions.

5.2.2. Ductility Coefficient. The damping ratio of 5% and the ductility coefficient of 1, 3, 5, and 8 are initially assumed based on the bilinear restoring force model. Figure 16 shows the influence of ductility coefficient on the hysteretic energy spectra under near-fault pulse-like and far-field harmonic ground motions. As the damping ratio of 5% keeps constant, the influencing rule of ductility coefficient on the hysteretic energy spectra under near-fault pulse-like ground motions is different from that under far-field harmonic ground motions. As the ductility coefficient increases, the peaks of hysteretic energy spectra drop under near-fault pulse-like ground motions, while the peaks of hysteretic energy spectra show a rising trend under far-field harmonic ground motions. The specific period corresponding to the peak both tends to the short-period direction under two types of long-period ground motions. For two types of long-period ground motions, ductility coefficient has little influence on the hysteretic energy spectra in the short period of 0–3 s, while the hysteretic energy spectra show a decreasing trend with the increase of ductility coefficient in the period range of 3–13 s. The hysteretic energy spectra are almost the same under different ductility coefficient, and the spectra values even tend to be stable when the vibration period is beyond 13 s.

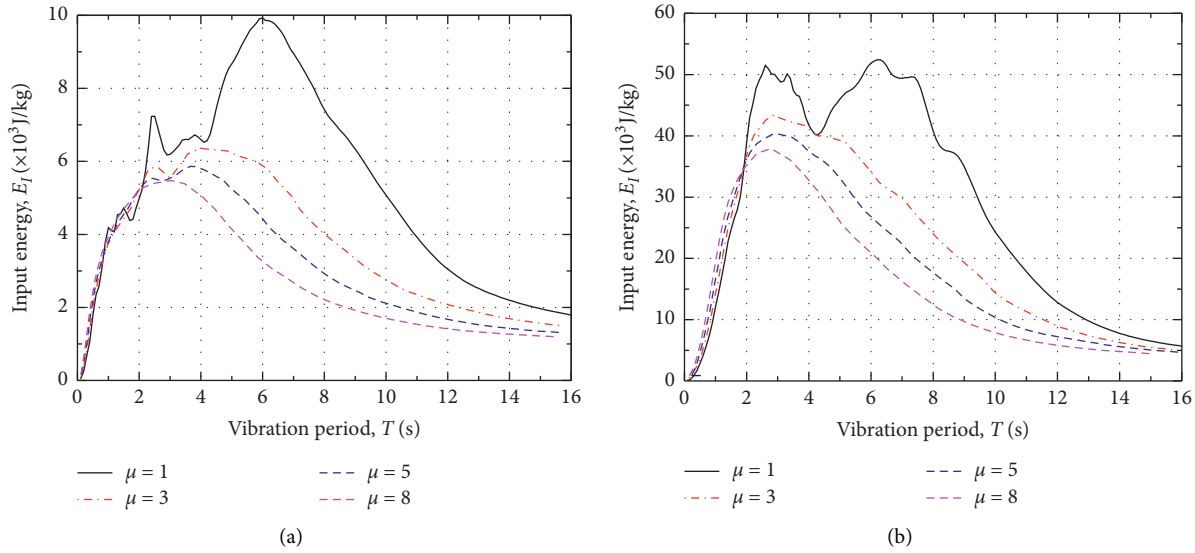

FIGURE 14: Input energy spectra affected by ductility coefficient. (a) Near-fault pulse-like ground motions. (b) Far-field harmonic ground motions.

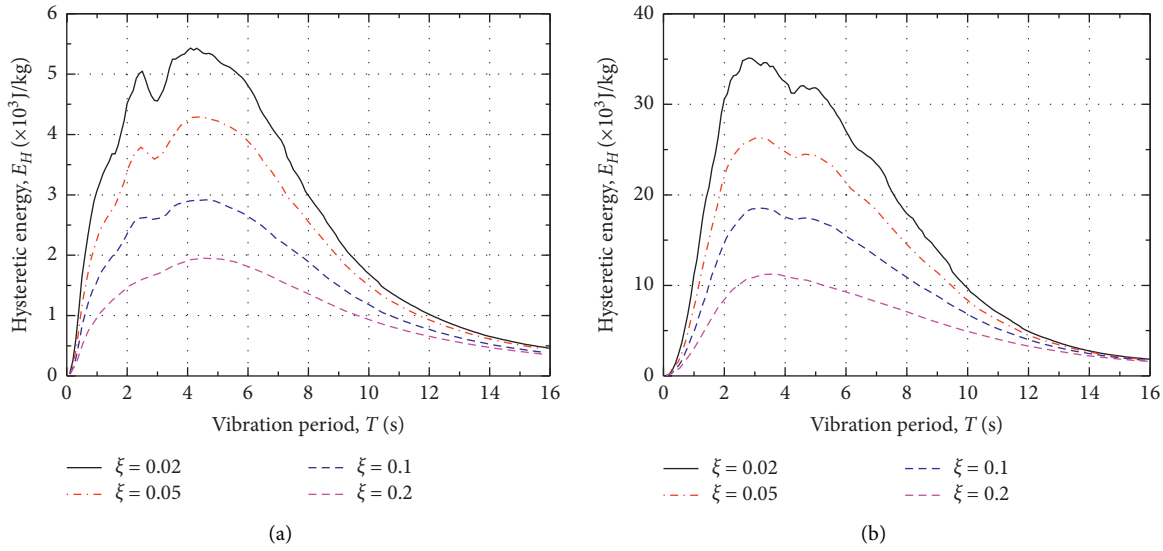

FIGURE 15: Hysteretic energy spectra affected by damping ratio. (a) Near-fault pulse-like ground motions. (b) Far-field harmonic ground motions.

5.2.3. Yield Stiffness Ratio. Bilinear restoring force models and stiffness degradation models are widely used for the hysteresis models of elastoplastic SDOF systems. The bilinear restoring force model is employed for this paper, and the yield stiffness ratio is the most important parameter influencing the bilinear restoring force models. The ductility coefficient of 3.0, the damping ratio of 5%, and the yield stiffness ratio of 0, 0.05, and 0.2 are initially assumed based on the bilinear restoring force model. Figure 17 shows the influence of yield stiffness ratio on the hysteretic energy spectra under near-fault pulse-like and far-field harmonic ground motions. As the ductility coefficient of 3.0 and damping ratio of 5% keep constant, the peaks of hysteretic energy spectra slightly grow with the increase of yield stiffness ratio under two types of long-period ground motions. As the yield stiffness ratio increases from 0, 0.05 to 0.2, the increasing amplitudes about the peaks of hysteretic energy spectra only reach 1.60% and 5.68% under near-fault pulse-like ground motions, while the increasing amplitudes about the peaks of hysteretic energy spectra only reach 3.96% and 7.30% under far-field harmonic ground motions.

In summary, the influence of yield stiffness ratio on the hysteretic energy can be neglected in the practical engineering application as the ductility coefficient and damping

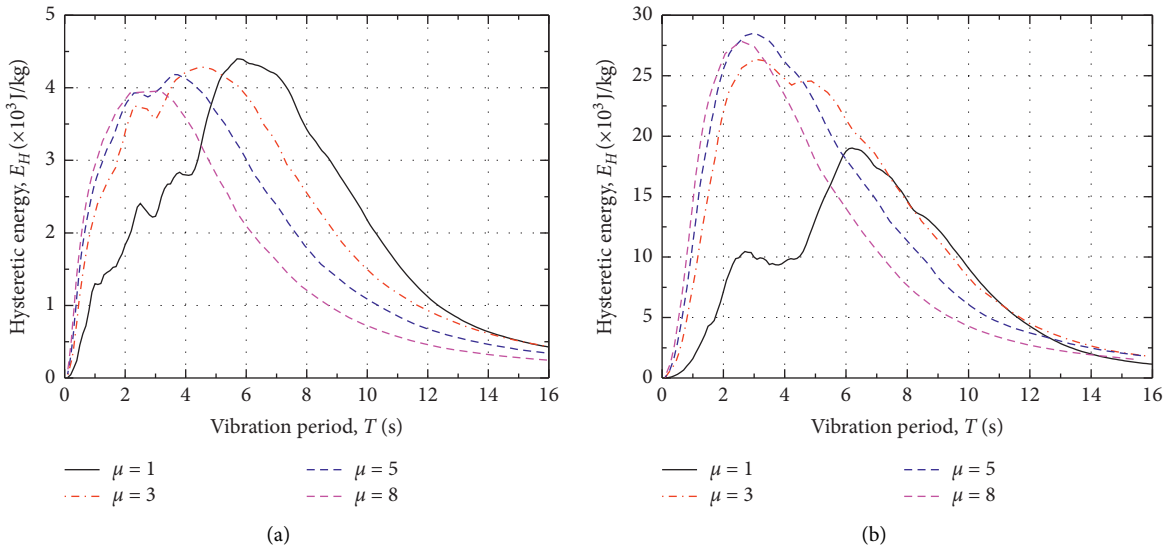

Figure 16: Hysteretic energy spectra affected by ductility coefficient. (a) Near-fault pulse-like ground motions. (b) Far-field harmonic ground motions.

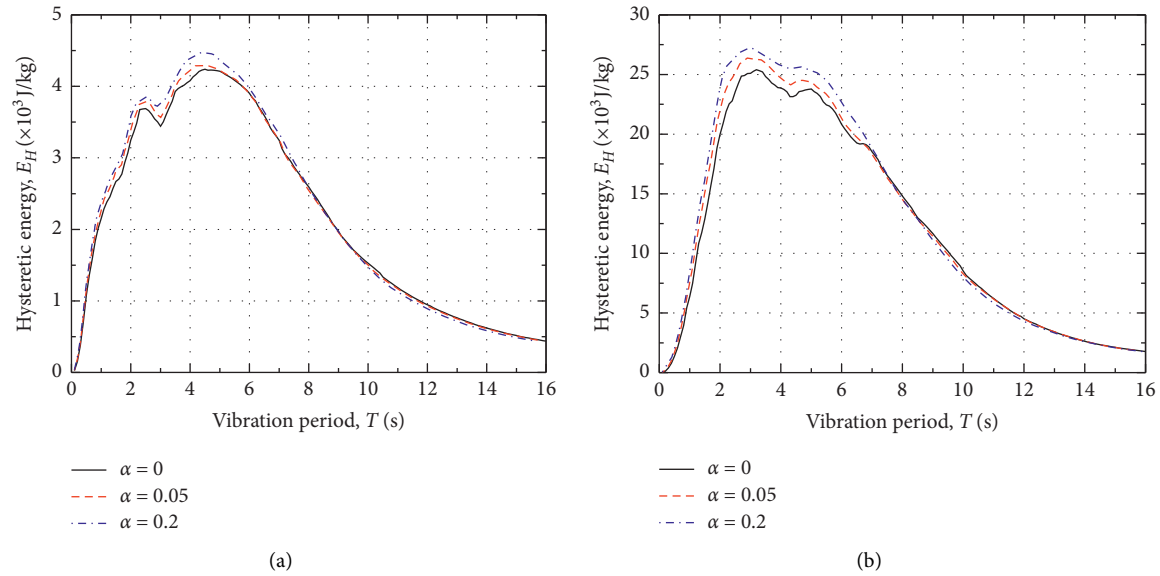

Figure 17: Hysteretic energy spectra affected by yield stiffness ratio. (a) Near-fault pulse-like ground motions. (b) Far-field harmonic ground motions.

ratio keep constant because yield stiffness ratio has little influence on the hysteretic energy under near-fault pulse-like and far-field harmonic ground motions.

6. Conclusions

The energy-based design method is used to evaluate the seismic energy response and energy distribution rule of elastoplastic SDOF systems under two types of special long-period earthquake excitation. The input energy, hysteretic energy, and damping energy are related to the characteristic of earthquake excitation and the dynamic characteristic of a structure itself, such as the earthquake magnitude, site condition, source-to-site distance, ductility coefficient, damping ratio, yield stiffness ratio, et al.

Within the whole period, all the input energy, hysteretic energy and damping energy spectra of SDOF systems under near-fault pulse-like and far-field harmonic ground motions, are larger than those under common ground motions, even the seismic energy response under far-field harmonic ground motions is larger than that under near-fault pulse-like ground motions. The peaks of input energy spectra, hysteretic energy spectra and damping energy spectra under long-period ground motions, show a rising trend with the

softer of site soil, and the increased amplifications even aggravate when the site soil gets softer. It is suggested to be related to the effects of filtering out the high-frequency components and amplifying the low-frequency components of soft site soil.

From the aspect of energy concept, the seismic energy response and energy distribution rule of SDOF systems are evaluated according to the intensity and spectral distribution under near-fault pulse-like and far-field harmonic ground motions. If the ratio of hysteretic energy to input energy (RHEIE) is determined, the hysteretic energy which must be dissipated by a structure would be derived by the method of energy-based design. The input energy and hysteretic energy are mainly influenced by damping ratio and ductility coefficient, while the yield stiffness ratio exerts minor effects. Therefore, the influence of yield stiffness ratio on the hysteretic energy can be neglected in the practical engineering application. It indicates that reasonable structural design parameters would contribute to the hysteretic energy of a structure itself.

Data Availability

No data were used to support this study.

Conflicts of Interest

The authors declare that they have no conflicts of interest regarding the publication of this paper.

Acknowledgments

The present work was supported by the Doctoral Research Foundation of Hubei University of Arts and Science (nos. 2059070), Project of Hubei University of Arts and Science, Hubei Superior and Distinctive Discipline Group of "Mechatronics and Automobiles," National Natural Science Foundation of China (no. 52074112), and Provincial Education Department Program of Hubei Province (no. D20182601). These supports were greatly appreciated.

References

[1] K. Koketsu and H. Miyake, "A seismological overview of long-period ground motion," *Journal of Seismology*, vol. 12, no. 2, pp. 133–143, 2008.

[2] I. Takewaki, S. Murakami, K. Fujita, S. Yoshitomi, M. Tsuji, and M. Tsuji, "The 2011 off the Pacific coast of Tohoku earthquake and response of high-rise buildings under long-period ground motions," *Soil Dynamics and Earthquake Engineering*, vol. 31, no. 11, pp. 1511–1528, 2011.

[3] Y. Cheng and G. L. Bai, "Basic characteristic parameters and influencing factors of long-period ground motion records," *Journal of Vibroengineering*, vol. 19, no. 7, pp. 5191–5207, 2017.

[4] Y.-L. Chung, T. Nagae, T. Hitaka et al., "Seismic resistance capacity of high-rise buildings subjected to long-period ground motions: E-Defense shaking table test," *Journal of Structural Engineering*, vol. 136, no. 6, pp. 637–644, 2010.

[5] T. Ariga, Y. Kanno, and I. Takewaki, "Resonant behaviour of base-isolated high-rise buildings under long-period ground motions," *The Structural Design of Tall and Special Buildings*, vol. 15, no. 3, pp. 325–338, 2006.

[6] F. Mazza, M. Mazza, and A. Vulcano, "Nonlinear response of r.c. framed buildings retrofitted by different base-isolation systems under horizontal and vertical components of near-fault earthquakes," *Earthquakes and Structures*, vol. 12, no. 1, pp. 135–144, 2017.

[7] F. Mazza, "Base-isolation of a hospital pavilion against in-plane-out-of-plane seismic collapse of masonry infills," *Engineering Structures*, vol. 228, Article ID 111504, 2021.

[8] R. S. Jalali and M. D. Trifunac, "A note on strength-reduction factors for design of structures near earthquake faults," *Soil Dynamics and Earthquake Engineering*, vol. 28, no. 3, pp. 212–222, 2008.

[9] A. K. Chopra and C. Chintanapakdee, "Inelastic deformation ratios for design and evaluation of structures: single-degree-of-freedom bilinear systems," *Journal of Structural Engineering*, vol. 130, no. 9, pp. 1309–1319, 2004.

[10] Y.-R. Dong, Z.-D. Xu, K. Zeng, Y. Cheng, and C. Xu, "Seismic behavior and cross-scale refinement model of damage evolution for RC shear walls," *Engineering Structures*, vol. 167, pp. 13–25, 2018.

[11] Y.-R. Dong, Z.-D. Xu, Q.-Q. Li, Y.-S. Xu, and Z.-H. Chen, "Seismic behavior and damage evolution for retrofitted RC frames using haunch viscoelastic damping braces," *Engineering Structures*, vol. 199, Article ID 109583, 2019.

[12] G. W. Housner, "Limit design of structures to resist earthquake," in *Proceedings of 1st World Conference on Earthquake Engineering*, vol. 5, pp. 5.1–5.13, Berkeley, CF, USA, July 1956.

[13] C.-M. Uang and V. V. Bertero, "Evaluation of seismic energy in structures," *Earthquake Engineering & Structural Dynamics*, vol. 19, no. 1, pp. 77–90, 1990.

[14] P. Fajfar and T. Vidic, "Consistent inelastic design spectra: hysteretic and input energy," *Earthquake Engineering & Structural Dynamics*, vol. 23, no. 5, pp. 523–537, 1994.

[15] G. Ghodrati Amiri, G. A. Darzi, and J. Vaseghi Amiri, "Design elastic input energy spectra based on Iranian earthquakes," *Canadian Journal of Civil Engineering*, vol. 35, no. 6, pp. 635–646, 2008.

[16] A. Benavent-Climent, F. López-Almansa, and D. A. Bravo-González, "Design energy input spectra for moderate-to-high seismicity regions based on Colombian earthquakes," *Soil Dynamics and Earthquake Engineering*, vol. 30, no. 11, pp. 1129–1148, 2010.

[17] S. Szyniszewski and T. Krauthammer, "Energy flow in progressive collapse of steel framed buildings," *Engineering Structures*, vol. 42, pp. 142–153, 2012.

[18] C. Zhai, Z. Chang, S. Li, Z. Chen, and L. Xie, "Quantitative identification of near-fault pulse-like ground motions based on energy," *Bulletin of the Seismological Society of America*, vol. 103, no. 5, pp. 2591–2603, 2013.

[19] K. Ke, G. Chuan, and S. Ke, "Seismic energy factor of self-centering systems subjected to near-fault earthquake ground motions," *Soil Dynamics and Earthquake Engineering*, vol. 84, pp. 169–173, 2016.

[20] S. Pathak, A. Khennane, and S. Al Deen, "Energy formulation for seismic collapse assessment of RCC structures: improvements in performance design," in *Proceedings of Australian Earthquake Engineering Society 2017*, Canberra, Australia, November 2017.

[21] D. Deniz, J. Song, and J. F. Hajjar, "Energy-based sidesway collapse fragilities for ductile structural frames under earthquake loadings," *Engineering Structures*, vol. 174, pp. 282–294, 2018.

[22] I. Takewaki and K. Fujita, "Earthquake input energy to tall and base-isolated buildings in time and frequency dual domains," *The Structural Design of Tall and Special Buildings*, vol. 18, no. 6, pp. 589–606, 2009.

[23] Q.-j. Chen, W.-z. Yuan, Y.-c. Li, and L.-y. Cao, "Dynamic response characteristics of super high-rise buildings subjected to long-period ground motions," *Journal of Central South University*, vol. 20, no. 5, pp. 1341–1353, 2013.

[24] L. D. Decanini and F. Mollaioli, "Formulation of elastic earthquake input energy spectra," *Earthquake Engineering & Structural Dynamics*, vol. 27, no. 12, pp. 1503–1522, 1998.

[25] H. Sucuoğlu and A. Nurtuğ, "Earthquake ground motion characteristics and seismic energy dissipation," *Earthquake Engineering and Structural Dynamics*, vol. 24, no. 9, pp. 1195–1213, 1995.

[26] H. Akiyama, "Collapse modes of structures under strong motions of earthquake," *Annals of Geophysics*, vol. 45, no. 6, pp. 791–798, 2002.

[27] N. Fukuwa and J. Tobita, "Key parameters governing the dynamic response of long-period structures," *Journal of Seismology*, vol. 12, no. 2, pp. 295–306, 2008.

[28] Y. Cheng, G. Bai, and Y. Dong, "Spectrum characterization of two types of long-period ground motions and seismic behavior of frame-core wall structures under multidimensional earthquake records," *The Structural Design of Tall and Special Buildings*, vol. 27, no. 16, p. e1539, 2018.

[29] J. Li, H. Zhou, and Y. Ding, "Stochastic seismic collapse and reliability assessment of high-rise reinforced concrete structures," *The Structural Design of Tall and Special Buildings*, vol. 27, no. 2, p. e1417, 2018.

[30] S. K. Shahi and J. W. Baker, "An efficient algorithm to identify strong-velocity pulses in multicomponent ground motions," *Bulletin of the Seismological Society of America*, vol. 104, no. 5, pp. 2456–2466, 2014.

[31] H. Choi and J. Kim, "Energy-based seismic design of buckling-restrained braced frames using hysteretic energy spectrum," *Engineering Structures*, vol. 28, no. 2, pp. 304–311, 2006.

[32] Z. F. Liu and P. S. Shen, "Evaluation of hysteretic energy to input energy ratio in tall hybrid structures," *Journal of Earthquake Engineering and Engineering Vibration*, vol. 29, no. 2, pp. 73–78, 2009.